Synthesis, Structure, Electronic Spectroscopy, Photophysics, Electrochemistry, and X-ray Photoelectron Spectroscopy of Highly-Electron-Deficient [5,10,15,20-Tetrakis(perfluoroalkyl)porphinato]zinc(II) Complexes and Their Free Base Derivatives

James G. Goll,[‡] Kevin T. Moore,[‡] Abhik Ghosh,[†] and Michael J. Therien*[,‡]

Contribution from the Departments of Chemistry, University of Pennsylvania, Philadelphia, Pennsylvania 19104-6323, and the Institute of Mathematical and Physical Sciences (IMR), University of Tromsø, Breivika, N-9037 Tromsø, Norway

Received April 2, 1996[⊗]

Abstract: The synthesis, optical spectroscopy, photophysical properties, electrochemistry, and X-ray photoelectron spectroscopy of a series of [5,10,15,20-tetrakis(perfluoroalkyl)porphinato]zinc(II) complexes and their free base analogs are reported. The title compounds were prepared by a condensation methodology that utilizes perfluoro-1-(2′-pyrrolyl)-1-alkanol precursors and employs continuous water removal throughout the course of the reaction to yield the *meso* perfluorocarbon-substituted porphyrins. The nature of the porphyrin-pendant *meso*-perfluoroalkyl group exerts considerable influence over the macrocycle's solubility properties. The structure of the monopyridyl adduct of [5,-10,15,20-tetrakis(heptafluoropropyl)porphinato]zinc(II) features an S_4-distorted porphyrin core; X-ray data are as follows: $P\bar{1}$ with $a = 15.1330(5)$ Å, $b = 19.2780(6)$ Å, $c = 14.6030(4)$ Å, $\alpha = 110.220(2)°$, $\beta = 103.920(2)°$, $\gamma = 85.666(2)°$, $V = 3880.1(2)$ Å^3, $d_{calc} = 1.887$ g cm^{-3}, and $Z = 4$. Electrochemical studies carried out on these porphyrin and (porphinato)zinc(II) complexes indicate that *meso*-perfluoroalkylporphyrins are among the most electron-deficient porphyrinic species known. X-ray photoelectron spectroscopy experiments corroborate the electron poor nature of these systems and evince extreme stabilization of the nitrogen 1s orbitals, consonant with particularly effective removal of electron density from the macrocycle by the *meso*-perfluoroalkyl moieties that is modulated by σ-symmetry orbitals. The photophysical properties of these compounds differ from all other previously reported highly electron deficient porphyrin macrocycles in that they possess long-lived, fluorescent excited states; hence their optoelectronic features are consistent with a variety of excited-state electron-transfer quenching schemes in which both ^{1}ZnP* and ^{1}H$_2$P* can be utilized as potent photooxidants.

Introduction

Recently, we reported methodology that readily enables the synthesis of 5,10,15,20-tetrakis(perfluoroalkyl)porphyrins.[1] In contrast to the extensively utilized, similarly electron deficient [2,3,7,8,12,13,17,18-octahalo-5,10,15,20-tetrakis(pentafluorophenyl)porphyrin ligand systems,[2] the tetrakis(*meso*-perfluoroalkyl)porphyrins can be directly synthesized in high yield from simple monopyrrolic precursors.[1] Furthermore, it was demonstrated that concentrated solutions of the 5,10,15,20-tetrakis-(heptafluoropropyl)porphyrin ligand could be obtained in both protic and aprotic polar solvents such as methanol and acetonitrile, as well as in low dielectric strength alkane and chlorofluorocarbon (CFC) media, underscoring the broad prospects for such a macrocycle in transition metal chemistry.

We present herein the first of several reports detailing the transition metal-based chemistry and physical properties of the 5,10,15,20-tetrakis(perfluoroalkyl)porphyrin ligand system, focusing on the synthesis, structure, electronic spectroscopy, elementary photophysics, and electrochemistry of a family of 5,10,15,20-tetrakis(perfluoroalkyl)porphyrins and their associated [porphinato]zinc(II) complexes. Furthermore, we report the first XPS measurements that detail the impact that the *meso*-perfluoroalkyl group has upon the electrostatic potential at the core nitrogen atoms and discuss how these experiments serve to illuminate the unusual electronic features of these porphyrin-based macrocyclic ligands. In addition to contrasting the physical properties of these compounds with those observed for traditional electron deficient porphyrins, we report how the simple variation of the length of the carbon chain of the *meso*-perfluoroalkyl moiety remarkably modulates the solubility properties of these systems.

Experimental Section

Materials. Inert atmosphere manipulations, as well as reagent and solvent purification, were carried as described previously.[1] Solvents utilized in this work were obtained from Fisher Scientific (HPLC Grade) or Aldrich Chemical (HPLC Grade). Perfluoroalkylaldehyde hydrates and perfluoroalkyl chlorides were obtained either from PCR Inc., Oakwood Chemicals, or Lancaster Synthesis. *p*-Toluenesulfonic acid (*p*-TsOH·H$_2$O) was obtained from Fisher Scientific. Triethylamine was dried over KOH and then vacuum transferred to a Schlenk storage tube. Molecular sieves (3 and 4 Å) were dried for a minimum of 12 h at 125 °C under vacuum. All other materials were used as received. Chromatographic purification (Silica Gel 60, 230-400 mesh, EM Science) of all newly synthesized porphyrins was accomplished on the bench top. [Porphinato]zinc complexes were chromatographically purified with neutral alumina (Brockmann Activity I, 60-325 Mesh,

‡ University of Pennsylvania.
† University of Tromsø.
⊗ Abstract published in *Advance ACS Abstracts,* August 1, 1996.
(1) DiMagno, S. G.; Williams, R. A; Therien, M. J. *J. Org. Chem.* **1994**, *59*, 6943−6948.
(2) (a) Traylor, T. G.; Tsuchiya, S. *Inorg. Chem.* **1987**, *26*, 1338−1339. (b) Lyons, J. E.; Ellis, P. E., Jr. *Catal. Lett.* **1991**, *8*, 45−52. (c) Bhyrappa, P.; Krishnan, V. *Inorg. Chem.* **1991**, *30*, 239−245. (d) Mandon, D.; Ochsenbein, P.; Fischer, J.; Weiss, R.; Jayaraj, K.; Austin, R. N.; Gold, A.; White, P. S.; Brigaud, O.; Battioni, P.; Mansuy, D. *Inorg. Chem.* **1992**, *31*, 2044−2049.

S0002-7863(96)01090-6 CCC: $12.00

Fisher Scientific). Chemical shifts for ^{1}H NMR spectra are relative to residual protium in the deuteriochloroform solvent ($CDCl_3$, $\delta = 7.24$ ppm). Chemical shifts for ^{19}F NMR spectra are relative to $CFCl_3$, $\delta = 0$ ppm. Mass spectra were obtained at the University of Pennsylvania Mass Spectrometry Laboratory. Elemental analyses were performed at Robertson Microlit Laboratories (Madison, NJ).

Instrumentation. Electronic spectra were recorded on an OLIS UV/vis/NIR spectrophotometry system that is based on the optics of a Cary 14 spectrophotometer. Emission spectra and quantum yields were determined using a Perkin-Elmer LS 50 luminescence spectrometer. Quantum yields were determined by established methods that utilized 5,10,15,20-tetraphenylporphyrin or [5,10,15,20-tetraphenylporphinato]-zinc(II) as standards.[3] NMR spectra were recorded on either a 200-MHz AM-200 or 250-MHz AC-250 Brüker spectrometer. Cyclic voltammetric measurements were carried out with a PAR 273 electrochemical analyzer and a single-compartment electrochemical cell. Fluorescence lifetime measurements were accomplished utilizing a time-correlated single-photon counting (TCSPC) spectroscopy, with an apparatus that has been described in detail elsewhere.[4] Data were analyzed using the Lifetime Program [Regional Laser and Biotechnology Laboratory (RLBL), University of Pennsylvania]. All time-resolved fluorescence data could be fit as single-exponential decays over 5 lifetimes, giving satisfactory χ^2 values as well as residual and autocorrelation function analyses.

XPS measurements were carried out using a Physical Electronics 5600 spectrometer that utilized monochromatized aluminum Kα radiation (power = 500 W), using experimental methods described previously.[5] The electronic spectra of the porphyrins remained unchanged after the XPS measurements, indicating that the samples were stable to at least several minutes of X-ray irradiation.

2,2,2-Trifluoro-1-(2′-pyrrolyl)ethanol. A 100-mL Schlenk flask equipped with a magnetic stirring bar was charged with trifluoromethylaldehyde hydrate (15 mL, 160 mmol). The perfluoralkylaldehyde hydrate was frozen and a nitrogen atmosphere was established. Pyrrole (6.0 mL, 87 mmol) was added via syringe followed by NaOH pellets (2.07 g, 51.8 mmol). The flask was shielded from light with aluminum foil, the mixture was stirred for 4 days at room temperature, following which the volatiles were removed. Water (50 mL) was then added, and the product was extracted with chloroform (4 × 50 mL). The organic layer was dried over $MgSO_4$ and the solvent was removed by flash evaporation. The resultant oil was dissolved in benzene (10 mL) and lyophilized yielding a slightly air- and light-sensitive tan powder (5.92 g, 35.7 mmol, 41.3%). NMR spectroscopy shows that a trace amount of a bis[1-(2′-pyrrolyl)]-2,2,2-trifluoroethanol is present as an impurity; the product, however, was sufficiently pure to be used in subsequent reactions without additional purification. ^{1}H NMR (250 MHz, $CDCl_3$): δ 8.51 (br, 1 H), 6.83 (m, 1 H), 6.29 (m, 1 H), 6.20 (m, 1 H), 5.05 (qt of d, 1H, $J_{HF} = 6.6$ Hz, $J_{HH} = 4.8$ Hz), 2.45 (d, 1H, $J_{HH} = 4.8$ Hz). ^{19}F NMR ($CDCl_3$): δ −88.0 (d, 3F). FAB MS: 166 (calcd 166).

2,2,3,3,4,4,4-Heptafluoro-1-(2′-pyrrolyl)-1-butanol. This compound was prepared by a slight modification of the previously reported procedure.[1] Pyrrole (40.0 mL, 577 mmol), heptafluorobutylaldehyde hydrate (16.0, 62.9 mmol), and NaOH pellets (8.57 g, 214 mmol) were stirred for 19 h. The resultant oil was dissolved in benzene and lyophilized yielding a slightly air- and light-sensitive tan powder (9.63 g, 36.3 mmol, 57.7%). ^{1}H NMR, (250 MHz, $CDCl_3$): δ 8.51 (br s, 1 H), 6.85 (m, 1H), 6.31 (m, 1 H), 6.21 (m, 1 H), 5.22 (ddd, 1 H, $J_{HF} = 16.6$ Hz, $J_{HF} = 7.7$ Hz, $J_{HH} = 4.8$ Hz), 2.45 (d, 1H, $J_{HH} = 4.8$ Hz). FAB MS: 265 (calcd 265).

2,2,3,3,4,4,5,5,6,6,7,7,8,8,8-pentadecafluoro-1-(2′-pyrrolyl)-1-octanol. Under a nitrogen atmosphere, a 500-mL round-bottomed flask equipped with a magnetic stirring bar was charged with pyrrole (3.7 mL, 53 mmol), triethylamine (9.0 mL, 64.6 mmol), and dry THF (250 mL) and cooled in an ice bath. Perfluorooctanoyl chloride (12.2 g, 28.2 mmol) was added via syringe with vigorous stirring over a period of 5 min. The reaction was allowed to warm to room temperature. After reacting for an additional 4 h, the solution was filtered through a medium porosity fritted funnel, and the volatiles were removed by flash evaporation. The residual oil was dissolved in 1:1 methanol: water (150 mL); $NaHCO_3$ (0.56 g) and $NaBH_4$ (4.1 g) were added and the mixture was stirred overnight. Additional $NaBH_4$ (1.0 g) was then added, and stirring continued for 2 h. The methanol was removed by flash evaporation and the product was extracted from the aqueous phase with diethyl ether (4 × 100 mL). The ether was dried over $MgSO_4$; evaporation of the solvent gave a brown solid (9.89 g, 21.3 mmol, 75% yield), which was further purified by recrystallization from toluene to yield white crystals. ^{1}H NMR (250 MHz, $CDCl_3$): δ 8.56 (br, 1 H), 6.86 (m, 1 H), 6.30 (m, 1 H), 6.20 (m, 1 H), 5.25 (dd, 1 H, ($J_{HF} = 16.8$ Hz), $J_{HF} = 7.5$ Hz), 2.61 (br, 1 H). FAB MS $(M + 1)^+$: 466 (calcd 466).

General Procedure for the Preparation of Tetrakis(*meso*-perfluoroalkyl)porphyrins. Reagent grade toluene (600 mL) and *p*-TsOH·H_2O were placed in a 1000-mL, two-necked, round-bottomed flask equipped with a recycling Dean-Stark trap connected to an efficient condenser. Once the Dean-Stark trap was charged with freshly-activated 4 Å molecular sieves, the system was brought under dry nitrogen and the solution refluxed for 2 h. The perfluoro-1-(2′-pyrrolyl)-1-alcohol, dissolved in 30 mL of dry solvent, was then added to the refluxing solution and allowed to react for 20 min. At this point, 2,3-dichloro-5,6-dicyanobenzoquinone (DDQ) was added, and the solution refluxed for an additional 10 min. After the addition of pyridine (2 mL), the solution was poured onto a 10 × 7 cm column packed with dry silica.

5,10,15,20-Tetrakis(trifluoromethyl)porphyrin. 2,2,2-Trifluoro-1-(2′-pyrrolyl)ethanol (335 mg, 2.02 mmol), *p*-TsOH·H_2O (106.5 mg), and DDQ (1.1 g) were utilized as reactants. The silica-packed column was washed with benzene until the eluant was colorless. After removal of the solvent under reduced pressure, the residue was absorbed on silica, loaded on a 15 × 2 cm silica column, and eluted using 10:1 hexanes:benzene. A red band was collected; following removal of volatiles, the compound was recrystallized by slow diffusion of CH_3OH into a CH_2Cl_2 solution, giving dark purple crystals. Isolated yield = 48.4 mg [16.5%, based on 335 mg of 2,2,2-trifluoro-1-(2′-pyrrolyl)-ethanol]. ^{1}H NMR (250 MHz, $CDCl_3$): δ 9.60 (s, 8 H), −2.08 (s, 2 H); ^{19}F NMR ($CDCl_3$): δ −38.41 (s, 3 F). Vis (CH_2Cl_2): 403 (5.08), 510 (3.97), 545 (3.97), 593 (3.67), 649 (4.00). CI MS: 582 (calcd 582). Anal. Calcd for $C_{24}H_{10}N_4F_{12}$: C, 49.50; H, 1.73; N, 9.62. Found: C, 49.53; H, 1.64; N, 9.33.

5,10,15,20-Tetrakis(heptafluoropropyl)porphyrin. 2,2,3,3,4,4,4-Heptafluoro-1-(2′-pyrrolyl)-1-butanol (503 mg, 1.90 mmol), *p*-TsOH·H_2O (119 mg), and DDQ (1.1 g) were utilized as reactants. The silica-packed column was washed with hexanes until the eluant was colorless. After removal of the solvent under reduced pressure, the residue was absorbed on silica, loaded on a 20 × 10 cm silica column, and eluted with 4:1 hexanes:CH_2Cl_2. A red band was collected; following removal of volatiles, the compound can be further purified by recrystallization from either hexanes or chloroform to give purple crystals. Isolated yield = 175.4 mg [37.6%, based on 503 mg of 2,2,3,3,4,4,4-heptafluoro-1-(2′-pyrrolyl)-1-butanol]. ^{1}H NMR (250 MHz, $CDCl_3$): δ 9.50 (s, 8 H), −2.32 (s 2 H). ^{19}F NMR ($CDCl_3$): δ −79.3 (br, 3 F), −79.8 (br, 2 F), −118.6 (br, 2 F). Vis (CH_2Cl_2): 405 (5.06), 510 (3.98), 544 (3.89), 593 (3.64), 647 (3.98).

5,10,15,20-Tetrakis(pentadecafluoroheptyl)porphyrin. 2,2,3,3,-4,4,5,5,6,6,7,7,8,8,8-pentadecafluoro-1-(2′-pyrrolyl)-1-octanol (1.54 g, 3.30 mmol), *p*-TsOH·H_2O (110 mg), and DDQ (1.6 g) were utilized as reactants. The silica-packed column was washed with 1,1,2-trichlorotrifluoroethane (1,1,2-$C_2Cl_3F_3$) until the eluant was colorless. After removal of the solvent under reduced pressure, the residue was absorbed on silica, loaded on a 12 × 6.5 cm silica column packed with CH_2Cl_2, and eluted with 1,1,2-$C_2Cl_3F_3$; following removal of the solvent, the compound was recrystallized from 1,1,2-$C_2Cl_3F_3$ and toluene to give dark purple crystals. Isolated yield = 505 mg [34.3% based on 1.54 g of 2,2,3,3,4,4,5,5,6,6,7,7,8,8,8-pentadecafluoro-1-(2′-pyrrolyl)-1-octanol]. ^{1}H NMR (250 MHz, $CDCl_3$, 1,1,2-$C_2Cl_3F_3$): δ

(3) (a) Harriman, A.; Davila, J. *Tetrahedron* **1989**, *45*, 4737−4750. (b) Fonda, H. N.; Gilbert, J. V.; Cormier, R. A.; Sprague, J. R.; Kamioka, K.; Connolly, J. S. *J. Phys. Chem.* **1993**, *97*, 7024−7033.

(4) The TCSPC apparatus has been described in detail elsewhere [Holtom, G. R. SPIE **1990**, *1204*, 1−12]. For these experiments, $\lambda_{ex} = 560$ nm; $\lambda_{em} = 600$ nm; instrument response function = 30 ps fwhm. Data were analyzed using Lifetime (RLBL) and Globals Unlimited (LFD, University of Illinois) Programs.

(5) Gassman, P. G.; Ghosh, A.; Almlöf, J. *J. Am. Chem. Soc.* **1992**, *114*, 9990−10000.

9.54 (s, 8 H), −2.25 (s 2 H); ^{19}F NMR ($CDCl_3$): δ −80.7, (br, 2 F), −82.3, (br, 3 F), −115.3, (br, 2 F), −121.7, (br, 2 F), −122.1, (br, 2 F), −122.8, (br, 2 F), −126.7, (br, 2 F). Vis (1,1,2-$C_2Cl_3F_3$): 403 (4.97), 508 (4.09), 541 (3.96), 593 (3.78), 647 (3.94). CI MS: 1783 (calcd 1783). Anal. Calcd for $C_{48}H_{10}N_4F_{60}$: C, 32.34; H, 0.57; N, 3.10. Found: C, 32.41; H, 0.71; N, 3.21.

General Procedure for the Preparation of [5,10,15,20-Tetrakis-(perfluoroalkyl)porphinato]zinc(II) Complexes. The tetrakis(*meso*-perfluoroalkyl)porphyrin was dissolved in an appropriate solvent and stirred with zinc acetate in the presence of triethylamine. After evaporation of the solvent, the product was purified by flash chromatography on alumina using THF as the eluant.

[5,10,15,20-Tetrakis(trifluoromethyl)porphinato]zinc(II). 5,10,-15,20-Tetrakis(trifluoromethyl)porphyrin (41.1 mg, 0.0706 mmol), Zn-$(OAc)_2$ (67.8 mg), and Et_3N (1 mL) were dissolved in 25 mL of $CHCl_3$ and allowed to react at room temperature for 8 h. The (porphinato)-zinc(II) product (33.2 mg) was isolated following chromatography (72.8%, based on 41.1 mg of the porphyrin starting material). Following recrystallization from THF, an analytical sample was prepared by heating the collected crystalline solid at 120 °C overnight under vacuum. ^{1}H NMR (250 MHz, $CDCl_3$): δ 9.78 (s, 8 H). ^{19}F NMR ($CDCl_3$): δ −36.48 (s, 3 F). Vis (CH_2Cl_2): 409 (5.27), 554 (3.99), 593 (4.29). CI MS: 644 (calcd 644). $(M - F)^+$: 625. $(M - CF_3)^+$: 575. Anal. Calcd for $C_{28}H_{16}N_4F_{12}OZn$: C, 44.64; H, 1.25; N, 8.68. Found: C, 44.51; H, 1.31; N, 8.39.

[5,10,15,20-Tetrakis(heptafluoropropyl)porphinato]zinc(II). 5,-10,15,20-Tetrakis (heptafluoropropyl)porphyrin (205.5 mg, 0.115 mmol), $Zn(OAc)_2$ (111.9 mg), and Et_3N (1 mL) were dissolved in 20 mL of $CHCl_3$ and allowed to react at room temperature for 1 h. The (porphinato)zinc(II) product (156.6 mg) was isolated following chromatography (73.8%, based on 205.5 mg of the porphyrin starting material). An analytical sample was recrystallized from THF. ^{1}H NMR (250 MHz, $CDCl_3$): δ 9.48 (s, 8 H). ^{19}F NMR ($CDCl_3$): δ −77.5 (br, 2 F), −79.7 (m, 3 F), −118.4 (br, 2 F). Vis (CH_2Cl_2): 409 (5.27), 553 (4.01), 592 (4.29). FAB MS: 1044 (calcd 1044). $(M - F)^+$: 1025. $(M - C_2F_5)^+$: 925. $(M - C_3F_7)^+$: 875. Anal. Calcd for $C_{36}H_{16}N_4F_{28}$-OZn: C, 38.68; H, 1.44; N, 5.01. Found: C, 38.47; H, 1.27; N, 5.09.

[5,10,15,20-Tetrakis(pentadecafluoroheptyl)porphinato]zinc-(II). 5,10,15,20-Tetrakis(pentadecafluoroheptyl)porphyrin (108.2 mg, 0.110 mmol), $Zn(OAc)_2$ (111.9 mg), and Et_3N (1 mL) were dissolved in 50 mL of 1,1,2-$C_2Cl_3F_3$ and allowed to react at room temperature for 8 h. The (porphinato)zinc(II) product (81.2 mg) was isolated following chromatography (70.6%, based on 108.2 mg of the porphyrin starting material). An analytical sample was recrystallized from THF. ^{1}H NMR (250 MHz, $CDCl_3$, 1,1,2-$C_2Cl_3F_3$): δ 9.59 (s, 8 H). ^{19}F NMR ($CDCl_3$): δ −77.5 (br, 2 F), −79.7 (t, 3 F), −118.4 (s, 2 F). Vis (THF): 417 (5.29), 558 (4.08), 597 (4.19). FAB MS: 1845 (calcd 1845). Anal. Calcd for $C_{52}H_{16}N_4F_{60}OZn$: C, 32.56; H, 0.84; N, 2.92. Found: C, 32.82; H, 0.97; N, 2.89.

X-ray Crystallography.[6] The crystal structure of [5,10,15,20-tetrakis(heptafluoropropyl)porphinato]zinc(II) was solved by direct methods (SIR92).[7] Details of crystal and data collection parameters are shown in Table 1. The structure was determined by Dr. Patrick Carroll at the Chemistry Department's X-ray Facility at the University of Pennsylvania.

[5,10,15,20-Tetrakis(heptafluoropropyl)porphinato]zinc(II)·Pyridine. Crystallization of the compound was induced by slow evaporation of a 99:1 acetonitrile:pyridine solution to yield translucent, rectangular red needles. The crystal dimensions were 0.070 × 0.15 × 0.42 mm. The pyridyl adduct of [5,10,15,20-tetrakis(heptafluoropropyl)porphinato]zinc(II) crystallizes in the triclinic space group $P\bar{1}$ with $a = 15.1330(5)$ Å, $b = 19.2780(6)$ Å, $c = 14.6030(4)$ Å, $\alpha = 110.220(2)°$, $\beta = 103.920(2)°$, $\gamma = 85.666(2)°$, $V = 3880.1(2)$ Å^3, $Z = 4$, and $d_{calc} = 1.887$ g/cm^3. X-ray intensity data were collected on an MSC/RAXIS IIc area detector employing graphite-monochromated Mo K_α radiation ($\lambda = 0.7107$ Å) at 235 K. A total of 27419 reflections were measured over the ranges: $4 \le 2\theta \le 50°$, $0 \le h \le 17$, $-22 \le k \le 22$, $-17 \le l \le 17$.

The intensity data were corrected for Lorentz and polarization effects but not for absorption. Of the reflections measured a total of 11991 unique reflections with $F^2 > 3\sigma(F^2)$ were used during subsequent structure refinement. Refinement was by full-matrix least-squares techniques based on F to minimize the quantity $\sum w(|F_o| - |F_c|)^2$ with $w = 1/\sigma^2(F)$. Non-hydrogen atoms were refined anisotropically and hydrogen atoms were refined isotropically. Refinement converged to $R_1 = 0.0752$ and $R_2 = 0.0860$.

Table 1. Summary of Structure Determination of [5,10,15,20-Tetrakis(heptafluoropropyl)porphinato]zinc(II)·Pyridine

formula	$ZnC_{37}H_{13}F_{28}N_5$
formula wt	1124.88
crystal class	triclinic
space group	$P\bar{1}$(No. 2)
Z	4
cell constants	
a	15.1330(5) Å
b	19.2780(6) Å
c	14.6030(4) Å
α	110.220(2)°
β	103.920(2)°
γ	85.666(2)°
V	3880.1(2) Å^3
μ	8.08 cm^{-1}
D_{calc}	1.887 g/cm^3
F(000)	2208.00
radiation	Mo K_α ($\lambda = 0.7107$ Å)
θ range	2.0−25.0°
h, *k*, *l* collected	+17, ±22, ±17
no. of reflcns meas	27419
no. of unique reflcns	11991 ($R_{merge} = 0.0588$)
no. of reflcns used in refinement	7319 ($F^2 > 3.0\sigma$)
no. of parameters	1271
data/parameter ratio	5.76
R_1	0.0752
R_2	0.0860
GOF	2.644

Results and Discussion

Synthesis, Solution Properties, and Structural Studies. As mentioned in our original report detailing the synthetic methodology to prepare 5,10,15,20-tetrakis(heptafluoropropyl)porphyrin [$(C_3F_7)_4PH_2$],[1] the approach is directly applicable to the fabrication of a variety of tetrakis(*meso*-perfluoroalkyl)porphyrins; the syntheses of 5,10,15,20-tetrakis(trifluoromethyl)porphyrin [$(CF_3)_4PH_2$] and 5,10,15,20-tetrakis(pentadecafluoroheptyl)-porphyrin [$(C_7F_{15})_4PH_2$] described in the Experimental Section represent two specific cases in point. These porphyrin systems were synthesized from their respective perfluoro-1-(2′-pyrrolyl)-1-alkanol precursors; implementation of acid-catalyzed condensation of these reagents in refluxing benzene or toluene, with the caveat that continuous water removal is required to build up significant quantities of the electron-deficient porphyrinogen in solution, enables the isolation of significant quantities of 5,-10,15,20-tetrakis(perfluoroalkyl)porphyrins upon oxidation. Yields of these materials are ∼35% for $R_f = (CF_2)_nCF_3$, when $n > 0$, and ∼15% for the $R_f = CF_3$ derivatives. More importantly, however, as exemplified by the preparation reported for 5,10,-15,20-tetrakis(pentadecafluoroheptyl)porphyrin, these syntheses can be carried out with sufficiently high concentrations of the perfluoro-1-(2′-pyrrolyl)-1-alkanol starting material to allow for the convenient isolation of over 1 g of the tetrakis(*meso*-perfluoroalkyl)porphyrin product from a single reaction using just over 1 L of solvent.

$(CF_3)_4PH_2$, $(C_3F_7)_4PH_2$, and $(C_7F_{15})_4PH_2$ exhibit solubility properties that are dependent upon the nature of their respective *meso*-perfluorocarbon groups, some of which are reflected in

(6) The atomic coordinates for this structure have been deposited with the Cambridge Crystallographic Data Centre. The coordinates can be obtained, on request, from the Director, Cambridge Crystallographic Data Centre, 12 Union Road, Cambridge, CB2 1EZ UK.

(7) Burla, M. C.; Camalli, M.; Cascarano, G.; Giacovazzo, C.; Polidori, G.; Spagna, R.; Viterbo, D. *J. Appl. Crystallogr.* **1989**, *72*, 389−393.

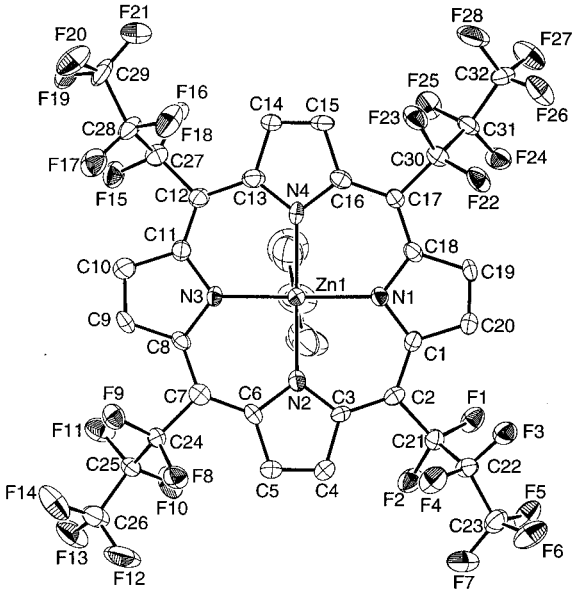

Figure 1. ORTEP view of the pyridyl adduct of [5,10,15,20-tetrakis-(heptafluoropropyl)porphinato]zinc(II) with thermal ellipsoids at the 30% probability.

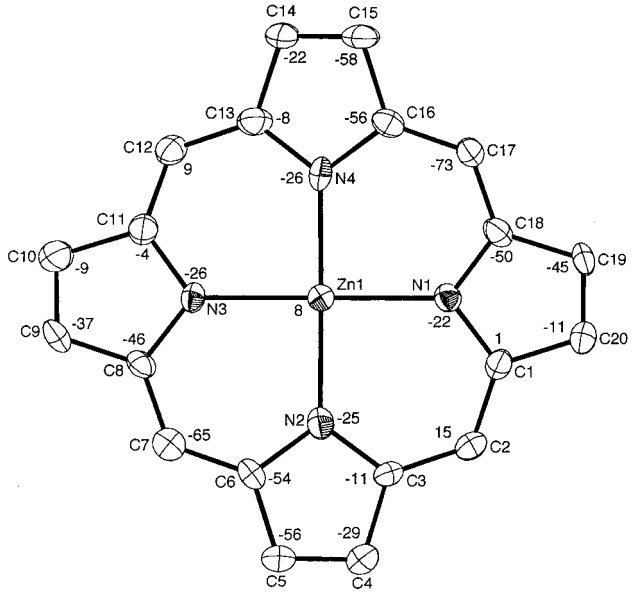

Figure 2. Diagrammatic representation of the porphyrin core of the pyridyl adduct of [5,10,15,20-tetrakis(heptafluoropropyl)porphinato]-zinc(II), illustrating the extent of the macrocycle S_4 distortion. The numbers adjacent to the atom labels signify the perpendicular displacements, in units of 0.01 Å, from the least-squares plane defined by the four porphyrin nitrogen atoms.

the disparate workup procedures for these compounds. $(C_7F_{15})_4PH_2$, for example, is insoluble in common organic solvents but dissolves readily in chlorofluorocarbon (CFC) and fluorocarbon solvents such as 1,1,2-trichlorotrifluoroethane and perfluoromethylcyclopentane. In contrast, $(CF_3)_4PH_2$ is totally insoluble in these types of halogenated solvents, but dissolves readily in a wide variety of organic media. As reported previously,[1] $(C_3F_7)_4PH_2$ dissolves in virtually any medium, and displays significant solubility in solvents that include pentane, aqueous methanol, CFC's, and fluorocarbons.

The 5,10,15,20-tetrakis(perfluoroalkyl)porphyrins can be metalated with zinc(II) under very mild conditions, merely by dissolving the macrocycle in an appropriate solvent with a simple zinc(II) salt in the presence of trialkylamine.[1] A structural study of one such electron-deficient (porphinato)zinc-(II) complex, the pyridyl adduct of [5,10,15,20-tetrakis(heptafluoropropyl)porphinato]zinc(II) [$(C_3F_7)_4PZn$], shows that there are two chemically identical, crystallographically independent molecules in the unit cell.[6] The major structural difference between these two species is largely manifest in the dihedral angel between the axial pyridine plane and the plane defined by a pair of opposite porphyrin $N_{pyrrolyl}$ atoms and the $N_{pyridyl}$ atom of the axial ligand (10.5 vs. 25.8°). For the sake of brevity, our discussion of the stereochemical features and metrical parameters of $(C_3F_7)_4PZn\cdot py$ will focus on just one of these crystallographically independent molecules.

Figure 1 shows an ORTEP view of the structure of $(C_3F_7)_4PZn\cdot py$ as viewed along the normal to the porphyrin plane. The structure displays a classic S_4 distortion; the magnitudes of the displacements of the Zn, $N_{pyrrolyl}$, C_α, C_{meso}, and C_β atoms from the least-squares plane defined by the four central porphyrinic nitrogens are represented in Figure 2. In contrast to DiMagno's recent report of the structure of the Co(II) derivative of the 5,-10,15,20-tetrakis(heptafluoropropyl)porphyrin ligand system, which is essentially saddle-distorted,[8] $(C_3F_7)_4PZn\cdot py$ adopts a ruffled structure similar to that observed for the free ligand,[1] though the degree of the S_4 distortion is much more severe, with the C_{meso} and C_β atoms alternately displaced on average 0.405 and 0.169 Å from the least-squares plane defined by the four central porphyrinic nitrogens.

As pointed out by Scheidt,[9] a primary driving force for ruffling of the porphyrin core is relief of steric strain at the periphery. The $(C_3F_7)_4PZn\cdot py$ structure shows eight short H−F nonbonded contacts involving the porphyrin β hydrogens and the fluorines that are attached to the perfluoropropyl carbon atoms bound directly to the porphyrin *meso*-carbon positions. These contacts range from 2.131 to 2.321 Å, and are well within the sum of the H and F van der Waals radii. These contacts would all be closer in a hypothetical planar structure for this molecule; hence, it is not surprising that the porphyrin adopts a significantly S_4-distorted configuration.[8,9] Because porphyrin core ruffling is enhanced with respect to that seen for the free ligand,[1] it is likely that the extremely electron deficient nature of the macrocycle also plays a key role in determining the extent of the S_4 distortion, since this also allows for reduced Zn−$N_{pyrrolic}$ bond distances with respect to what could be attained in a planar porphyrin structure.[9]

It is interesting to compare and contrast various aspects of this structure with other crystallographically characterized (porphinato)zinc(II)·pyridine complexes.[10] Of these, only a derivative of [5,10,15,20-tetraphenylporphinato]zinc(II) with a covalently attached pyridine ligand adopts a S_4-distorted structure,[10c] displaying modest average displacements of the C_{meso} and C_β atoms (0.203 and 0.094 Å, respectively) from the porphyrin least-squares plane. Tables 2A and 2B list selected bond distances and angles for the [tetrakis(*meso*-perfluoropropyl)porphinato]zinc(II) structure. The Zn−$N_{pyrrolic}$ bond distances (2.054−2.066 Å) are within the range of that reported for other (porphinato)zinc(II)·pyridine complexes (2.052−2.076 Å). The Zn−$N_{pyridyl}$ distance is short (2.140 Å), falling just

(8) DiMagno, S. G.; Wertsching, A. K.; Ross, C. R., II *J. Am. Chem. Soc.* **1995**, *117*, 8279−8280.

(9) Scheidt, W. R.; Lee, Y. J. *Struct. Bonding* **1987**, *64*, 1−70.

(10) (a) Collins, D. M.; Hoard, J. L. *J. Am. Chem. Soc.* **1970**, *92*, 3761−3771. (b) Cullen, D. L.; Meyer, E. F., Jr. *Acta. Crystallogr.* **1976**, *B32*, 2259−2269. (c) Bobrik, M. A.; Walker, F. A. *Inorg. Chem.* **1980**, *19*, 3383−3390. (d) Hatano, K.; Kawasaki, K.; Munakata, S.; Iitaka, Y. *Bull. Chem. Soc. Jpn.* **1987**, *60*, 1985−1992. (e) Barkigia, K. M.; Berber, M. D.; Fajer, J.; Medforth, C. J.; Renner, M. W.; Smith, K. M. *J. Am. Chem. Soc.* **1990**, *112*, 8851−8857. (f) Senge, M. O.; Eigenbrot, C. W.; Brennan, T. D.; Shusta, J.; Scheidt, W. R.; Smith, K. M. *Inorg. Chem.* **1993**, *32*, 3134−3142. (g) DiMagno, S. G.; Lin, V. S.-Y.; Therien, M. J. *J. Org. Chem.* **1993**, *58*, 5983−5993.

Table 2. Selected Bond Distances and Angles for [5,10,15,20-Tetrakis(perfluoropropyl)porphinato]zinc(II)

(A) Distance

bond	distance, Å	bond	distance, Å
Zn_1-N_1	2.066(7)	N_4-C_{13}	1.360(11)
Zn_1-N_2	2.068(8)	N_4-C_{16}	1.388(11)
Zn_1-N_3	2.057(7)	C_1-C_2	1.397(12)
Zn_1-N_4	2.054(8)	C_1-C_{20}	1.435(13)
Zn_1-N_5	2.140(8)	C_2-C_{21}	1.506(12)
F_1-C_{21}	1.346(10)	$C_{13}-C_{14}$	1.447(13)
F_2-C_{21}	1.351(10)	$C_{14}-C_{15}$	1.297(14)
N_1-C_1	1.380(10)	$C_{15}-C_{16}$	1.453(13)
N_1-C_{18}	1.374(11)	$C_{18}-C_{19}$	1.452(13)
		$C_{19}-C_{20}$	1.333(13)

(B) Angles

angle	angle, deg	angle	angle, deg
$N_1-Zn_1-N_2$	88.3(3)	$N_1-C_1-C_{20}$	108.5(8)
$N_1-Zn_1-N_3$	162.0(3)	$C_2-C_1-C_{20}$	126.5(9)
$N_1-Zn_1-N_5$	97.5(3)	$C_1-C_2-C_3$	125.3(8)
$N_2-Zn_1-N_5$	100.1(3)	$C_1-C_2-C_{21}$	118.4(9)
$Zn_1-N_1-C_1$	124.4(6)	$C_1-C_{20}-C_{19}$	108.3(9)
$Zn_1-N_1-C_{18}$	127.8(6)	$F_1-C_{21}-F_2$	104.2(7)
$C_1-N_1-C_{18}$	107.3(7)	$C_2-C_{21}-C_{22}$	117.0(8)
$N_1-C_1-C_2$	124.4(8)	$F_3-C_{22}-F_4$	106.5(8)

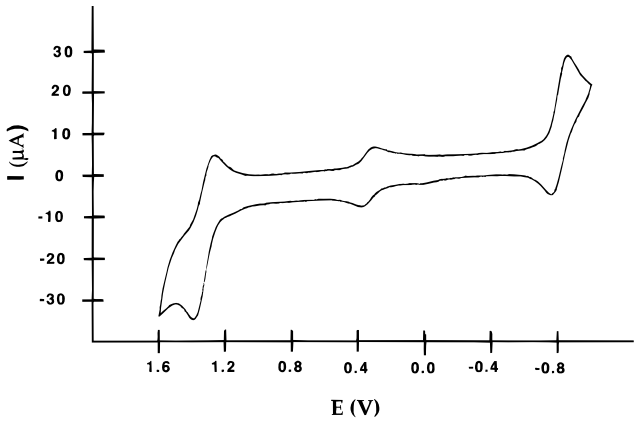

Figure 3. Cyclic voltammogram of [5,10,15,20-tetrakis(trifluoromethyl)porphinato]zinc(II) recorded in benzonitrile solvent showing the first anodic and cathodic redox processes. The redox process at 0.43 V vs SCE corresponds to the ferrocene/ferrocenium redox couple, which served as an internal potentiometric standard in our cyclic voltammetric studies. Experimental conditions are listed in Table 3.

outside the Zn-to-axial pyridine bond distance domain observed previously (2.143−2.220 Å);[10] the extent of zinc displacement, however, from the least-squares plane defined by the four central porphyrinic nitrogens is 0.33 Å and typical with respect to that seen in these other (porphinato)zinc(II)·pyridine structures.

Electrochemical Studies. 5,10,15,20-Tetrakis(perfluoroalkyl)porphyrins [$(R_f)_4PH_2$] and [5,10,15,20-tetrakis(perfluoroalkyl)porphinato]zinc(II) [$(R_f)_4PZn$] complexes exhibit current vs potential profiles characteristic of what has been traditionally observed in cyclic voltammetric studies of porphyrin and (porphinato)zinc(II) species at platinum or glassy carbon working electrode surfaces.[2c,11−12] Figure 3 shows the cyclic voltammetric response obtained for a benzonitrile solution of $(CF_3)_4PZn$. As is commonly observed for *meso*-substituted (porphinato)zinc(II) complexes, the initial anodic and cathodic electrode-coupled processes for $(R_f)_4PZn$ are one electron in nature and exhibit non-Nernstian, chemically reversible electrochemical behavior ($E_{pa} - E_{pc} > 58$ mV; $i_{pa}/i_{pc} \sim 1$) typical for (porphinato)metal ring-centered oxidations and reductions in nonaqueous solvent. Table 3 lists cyclic voltammetric data obtained for both the $(R_f)_4PH_2$ and $(R_f)_4PZn$ species examined in this study.

The free-base *meso*-perfluoroalkylporphyrins (Table 3) display only chemically reversible reductions. Cyclic voltammetric experiments carried out with $(CF_3)_4PH_2$ and $(C_3F_7)_4PH_2$ in THF show that these complexes undergo one-electron reductions at potentials approximately 0.92 V lower than the Fe(II/III) potential of ferrocene. The trifluoromethyl derivative is 40 mV more difficult to reduce than the analogous tetrakis(heptafluoropropyl)porphyrin, consistent with the longer chain perfluoroalkyl *meso* substituent having marginally more electron withdrawing power. $(C_7F_{15})_4PH_2$, being soluble only in fluorocarbon media, did not permit further comparison of the H_2P/H_2P^- redox potential as a function of the size of the *meso*-perfluoroalkyl group in a common solvent (THF).

Though soluble in a wide range of media, benzonitrile was the only solvent for the $(R_f)_4PZn$ complexes having appropriate dielectric strength as well as the reductive and oxidative stability required to examine both the initial anodic and cathodic redox processes. Similar to the electrochemical properties of $(C_3F_7)_4PZn$,[1] the cyclic voltammetric response of $(CF_3)_4PZn$ recorded in benzonitrile shows a ring-centered oxidation at 1440 mV, close to that observed for the dodeca-substituted [2,3,7,8,12,13,17,18-octabromo-5,10,15,20-tetrakis(pentafluorophenyl)porphinato]zinc(II) ($Br_8TFPPZn$)[1,2c,12] (1560 mV), and a ring-centered reduction at −710 mV, a potential 240 mV lower than the analogous electrode-coupled ZnP/ZnP^- reduction occurring at $Br_8TFPPZn$. While the limited solubility of $(C_7F_{15})_4PZn$ in benzonitrile precludes a comparison of both the one-electron oxidation and reduction potentials for all the compounds of the $(R_f)_4PZn$ series as a function of the nature of the perfluoroalkyl moiety in a single solvent, all three complexes are soluble in THF. Table 3 displays the reductive electrochemical data collected for the $(R_f)_4PZn$ complexes. In contrast to what was seen in the cathodic cyclic voltammetric responses for the $(R_f)_4PH_2$ compounds, it appears that the reduction potential of the $(R_f)_4PZn$ species drops slightly with increasing *meso*-perfluorocarbon chain length. Although this behavior was unexpected, these small observed perturbations of the ZnP/ZnP^- reduction potential may derive from disparate degrees of porphyrin ring ruffling in solution, or differences in the nature of solvation of the ZnP/ZnP^- species and axial ligand binding within the $(CF_3)_4PZn$, $(C_3F_7)_4PZn$, $(C_7F_{15})_4PZn$ series.

It is interesting to contrast the electrochemical behavior of $(R_f)_4PZn$ complexes with comparably electron-deficient $Br_8TFPPZn$. As demonstrated by Gray,[12] $Br_8TFPPZn$ exhibits two one-electron cathodic redox processes along with a single anodic process that is two electron in nature. Analysis of time-dependent spectroelectrochemical data was consistent with a mechanism in which the initially-formed $Br_8TFPPZn^+$ disproportionates into $Br_8TFPPZn$ and $Br_8TFPPZn^{2+}$; this anodic signature was interpreted as deriving from conformationally-induced destabilization of the HOMO in the dodeca-substituted porphyrins.[12,13] An alternative explanation for this behavior, however, stems from the types of conjugative interactions peculiar to severely saddle-distorted 2,3,7,8,12,13,17,18-octahalo-5,10,15,20-tetraarylporphyrin structure. The saddle struc-

(11) (a) Felton, R. H. In *The Porphyrins*, Dolphin, D., Ed.; Academic Press: London, 1979; Vol. V, pp 53−125. (b) Davis, D. G. In *The Porphyrins*, Dolphin, D., Ed.; Academic Press: London, 1979; Vol. V, pp 127−152. (c) Kadish, K. M. *Prog. Inorg. Chem.* **1986**, *34*, 435−605.

(12) Hodge, J. A.; Hill, M. G.; Gray, H. B. *Inorg. Chem.* **1995**, *34*, 809−812.

(13) (a) Takeuchi, T.; Gray, H. B.; Goddard, W. A., III *J. Am. Chem. Soc.* **1994**, *116*, 9730−9732. (b) Brigaud, O.; Battioni, P.; Mansuy, D. *New J. Chem.* **1992**, *16*, 1031−1038.

Table 3. Cyclic Voltammetric Data[a] for [5,10,15,20-Tetrakis(perfluoroalkyl)porphinato]zinc(II) Complexes and Their Free Base Analogues

Potentiometric Data (mV)										
	ZnP/ZnP$^+$				ZnP/ZnP$^-$					
compd	E_{pa}	E_{pc}	ΔE_p	$E_{1/2}$	E_{pa}	E_{pc}	ΔE_p	$E_{1/2}$	solvent	working electrode
$(CF_3)_4$PZn	1503	1377	126	1440	−659	−759	100	−709	PhCN	Pt
$(C_3F_7)_4$PZn[b]	1512	1407	105	1460	−685	−756	71	−720	PhCN	Pt
$(CF_3)_4$PZn					−496	−758	262	−627	THF	GC
$(C_3F_7)_4$PZn					−527	−811	284	−669	THF	GC
$(C_7F_{15})_4$PZn					−448	−908	460	−678	THF	GC
Potentiometric Data (mV)										
	H_2P/H_2P^+				H_2P/H_2P^-					
compd	E_{pa}	E_{pc}	ΔE_p	$E_{1/2}$	E_{pa}	E_{pc}	ΔE_p	$E_{1/2}$	solvent	working electrode
$(CF_3)_4PH_2$					−321	−481	160	−401	THF	Pt
$(C_3F_7)_4PH_2$					−282	−440	158	−361	THF	Pt

[a] Experimental conditions: [porphyrin] = 5 mM; [TBAPF$_6$] = 0.1 M; scan rate = 0.1 V/s; reference electrode = Ag wire. $E_{1/2}$ values reported are relative to SCE; the ferrocene/ferrocenium redox couple (0.43 V vs SCE, benzonitrile; 0.54 V vs SCE, THF) was used as the internal standard. [b] See ref 1.

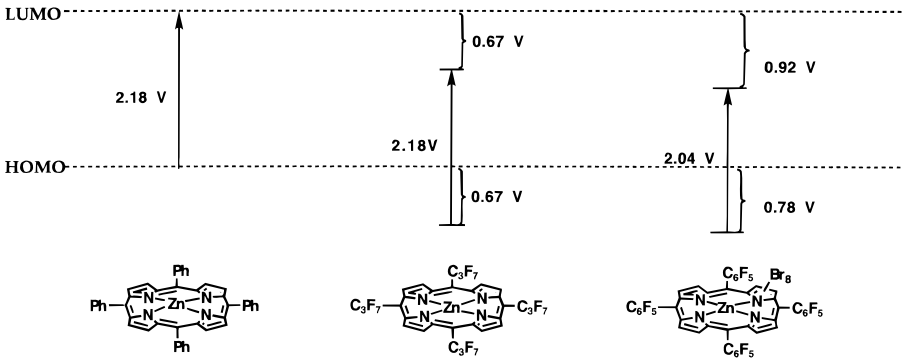

Figure 4. Relative HOMO/LUMO ($\pi-\pi^*$) gaps for [5,10,15,20-tetraphenylporphinato]zinc(II), [5,10,15,20-tetrakis(heptafluoropropyl)porphinato]-zinc(II), and [2,3,7,8,12,13,17,18-octabromo-5,10,15,20-tetrakis(pentafluorophenyl)porphinato]zinc(II) determined from cyclic voltammetric experimental data.

ture enables significantly enhanced porphyrin-to-*meso* phenyl π overlap with respect to that possible for a planar porphyrin structure; hence, it is likely that the extent of this electronic interaction is dependent upon the metalloporphyrin redox state. Because a disproportionation mechanism requires both Br$_8$-TFPPZn and Br$_8$TFPPZn^{2+} to be more stable than Br$_8$TFPPZn$^+$, it is reasonable to hypothesize that the dication and the monocation are not structurally isomorphous, with Br$_8$TFPPZn^{2+} having enhanced conjugative interactions with its pendant *meso*-fluorophenyl rings with respect to Br$_8$TFPPZn and Br$_8$TFPPZn$^+$. Such an explanation would be consistent with DiMagno's analysis of the optical and structural data obtained for [5,10,-15,20-tetrakis(heptafluoropropyl)porphinato]cobalt(II),[8] in which both experiment and theory show that red shifts in the porphyrin B and Q bands are not intrinsic to macrocycle distortion, but derive from disparate substituent effects for the *meso*-pendant groups in planar and nonplanar porphyrin conformations. We conclude that $(R_f)_4$PZn complexes likely have potentiometrically well-separated ZnP/ZnP$^+$ and ZnP$^+$/ZnP^{2+} redox couples since the *meso* substituents for these species are non-conjugating and effect electron removal from the porphyrin via the σ-bonding network, and thus cannot exhibit differential π overlap with the porphyrin core as a function of net metalloporphyrin-localized charge. For all the solvents examined in our electrochemical studies, however, the ZnP$^+$/ZnP^{2+} redox process lies at or beyond the anodic breakdown potential of the medium, thus prohibiting the evaluation of the ZnP/ZnP$^+$ → ZnP$^+$/ZnP^{2+} potential splitting.

Figure 4 summarizes some of this electrochemical data and displays the relative energies of the frontier molecular orbitals for these compounds along with their respective HOMO-LUMO ($\pi-\pi^*$) gaps determined from our cyclic voltammetric experiments. In contrast to the relationship of the electrochemically determined HOMO-LUMO gap for Br$_8$TFPPZn with respect to that observed for [5,10,15,20-tetraphenylporphinato]zinc(II) (TPPZn), Figure 4 emphasizes that the $\pi-\pi^*$ gap for $(R_f)_4$PZn complexes is unperturbed relative to TPPZn and underscores the fact that non-π conjugating perfluoroalkyl group substituents stabilize the porphyrin HOMO and LUMO to the same degree.

X-ray Photoelectron Spectroscopy. The electron-withdrawing ability of the *meso*-perfluoroalkyl group can also be assessed via core-level X-ray photoelectron spectroscopy (XPS),[5,14] which provides an important complement to electrochemical studies. While electrochemical oxidation produces π-delocalized cations in extended aromatic systems such as porphyrins, XPS core ionization produces atomic-centered holes; shifts in XPS core ionization potentials (IPs) thus reflect the electrostatic potentials at specific atomic sites.

Carbon 1s XPS spectra (data not shown) highlight the dramatically different core carbon ionization potentials of the CF_3 (292.7 eV), $CF_2CF_2CF_3$ (293.5 and 291.1 eV), and C_6F_5 (288.1 eV) groups and underscore the disparate σ-electron withdrawing power of the these three porphyrin *meso* substituents. How these fluorocarbon moieties impact the ligand properties of the porphyrin macrocycle can best be evaluated from the N 1s IP data (Figures 5A−C). From our XPS experimental results listed in Table 4, which compiles the nitrogen 1s IPs for the TFPPH$_2$, $(CF_3)_4PH_2$, and $(C_3F_7)_4PH_2$ ligands as well as the N 1s and Zn 2p$_{3/2}$ IPs for their associated

(14) (a) Ghosh, A.; Fitzgerald, J.; Gassman, P. G.; Almlöf, J. *Inorg. Chem.* **1994**, *33*, 6057−6060. (b) Ghosh, A. *J. Am. Chem. Soc.* **1995**, *117*, 4691−4699.

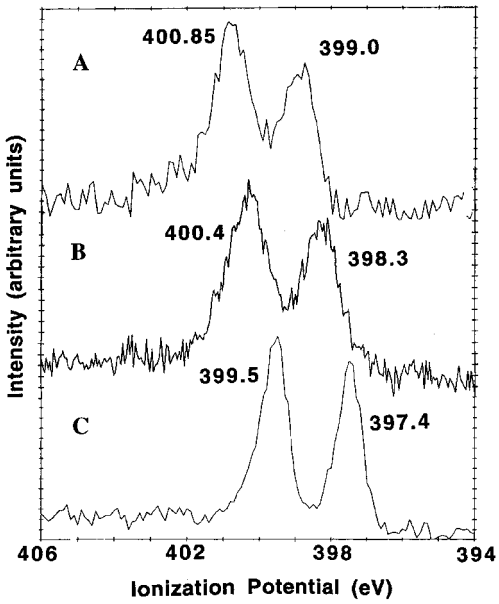

Figure 5. Nitrogen 1s XPS of (A) 5,10,15,20-tetrakis(heptafluoropropyl)porphyrin, (B) 5,10,15,20-tetrakis(trifluoromethyl)porphyrin, and (C) 5,10,15,20-tetrakis(pentafluorophenyl)porphyrin.

Table 4. XPS Core Ionization Potentials as a Function of Porphyrin and (Porphinato)zinc(II) *meso* Substituents

	ionization potentials (eV)			ionization potentials (eV)	
porphyrin	N1 1s	N2 1s	(porphinato)zinc(II) complex	N 1s	Zn $2p_{3/2}$
$TPPH_2$[a]	397.4	399.5	TPPZn	397.9	1021.5
$TFPPH_2$[a]	398.3	400.4	TFPPZn	398.5	1022.1
Br_8TPPH_2[b]	397.75	399.9			
$(CF_3)_4PH_2$	398.8	400.8	$(CF_3)_4PZn$	398.8	1022.4
$(C_3F_7)_4PH_2$	399.0	400.9	$(C_3F_7)_4PZn$	398.9	1022.5

[a] See ref 5. [b] See ref 14b.

(porphinato)zinc(II) complexes TFPPZn, $(CF_3)_4PZn$, and $(C_3F_7)_4PZn$, it is apparent that the nitrogen core (N1 1s) IPs of $(CF_3)_4PH_2$ (398.8 eV) and $(C_3F_7)_4PH_2$ (399.0 eV) exceed those of 5,10,15,20-tetraphenylporphyrin ($TPPH_2$) by 1.4 and 1.6 eV, respectively. (Note that a free base porphyrin has two symmetry-distinct nitrogen atoms; they are denoted as N1 and N2 in Table 4, and refer respectively to the unprotonated and protonated porphyrin-ring nitrogens.) Similar differences are manifest between the N2 1s IPs of these compounds as well.

To place the magnitude of these enormous substituent effects in perspective, Table 4 displays the nitrogen core ionization potential of 2,3,7,8,12,13,17,18-octabromo-5,10,15,20-tetraphenylporphyrin (Br_8TPPH_2) in addition to $TFPPH_2$. Note that perfluorination of all the phenyl rings of $TPPH_2$ results in an increase of only 0.9 eV in the IP of the N1 1s and N2 1s nitrogens while bromination of all the macrocycle β positions of $TPPH_2$ enhances the magnitude of the nitrogen core IPs on average by 0.38 eV. Making the first-order assumption that these effects should be additive,[15] we estimate N1 1s and N2 1s IPs for Br_8TFPPH_2 on the order of 398.65 and 400.8 eV, respectively. The tetrasubstituted porphyrin $(CF_3)_4PH_2$ is thus predicted to exhibit nitrogen core ionization potentials at least as large as those of Br_8TFPPH_2, which bears twelve electron-withdrawing groups. In any event, the N1 and N2 core ionization potentials for $(C_3F_7)_4PH_2$ are at least 0.35 and 0.1 eV larger, respectively, than any other porphyrin yet examined by this technique.

While *ab initio* Hartree−Fock and local density functional calculations predicted that the nitrogen core IPs of $(CF_3)_4PH_2$ should exceed those of $TPPH_2$ by 1.80 and 1.74 eV, respectively,[5,14b] it is important to point out that the results of our XPS experiments are congruent with that expected from first principles. As pointed out originally by Taft, Swain, and Lupton,[16] when substituent resonance effects are taken into account in aromatic systems with electron-demanding transition states, the trifluoromethyl group is superior to both the halogens and perfluorophenyl groups in terms of its electron-withdrawing ability. This derives from the significant inductive properties of the CF_3 moiety which are uncompensated by resonance effects; thus, when bound to the carbon framework of an aromatic system, the CF_3 group manifests relatively high σ_p and σ_p^+ values. Because substituent inductive effects are transmitted via the σ-bond network, it follows that the *meso*-perfluoroalkyl group should dramatically impact the electrostatic potential of the porphyrin central nitrogens. Consistent with this, our XPS results clearly indicate that $(R_f)_4PH_2$ *species should have remarkably different ligand properties* with respect to $TFPPH_2$ and Br_8TPPH_2; furthermore, while Br_8TFPPH_2 might be expected to have nitrogen core ionization potentials approaching those observed for $(R_f)_4PH_2$ compounds (*vide supra*), these severely saddle-distorted porphyrins provide a ligand environment distinct from *meso*-(perfluoroalkyl)-substituted porphyrins. Metal complexes of $(R_f)_4PH_2$ macrocycles will have significantly stabilized d orbitals with respect to their analogous $TPPH_2$ derivatives; moreover, the magnitude of stabilization of the $d_{x^2-y^2}$ and d_{z^2} orbitals will be exceptionally pronounced. Such d orbital electronic perturbations in $(R_f)_4PM$ systems will be manifest in both the chemical and optoelectronic characteristics of these species, influencing diverse properties such as metal-centered redox potential, the nature of metal-to-ligand and ligand-to-metal charge transfer interactions, ground- and excited-state electron spin distribution, and small molecule binding. Other work completed to date shows that this is indeed the case.[17]

That the *meso*-perfluoroalkyl group does influence the electrostatic potential of the porphyrin central metal atom is demonstrated by the data in Table 4; while perfluorination of the phenyl rings of TPPZn increases the Zn $2p_{3/2}$ IP by 0.6 eV, replacing the *meso*-phenyl moieties with perfluoroalkyl groups increases the Zn $2p_{3/2}$ IP by 1.0 eV. It is also interesting to note that while the magnitude of N 1s IP of both $(CF_3)_4PZn$ and $(C_3F_7)_4PZn$ is identical to the N1 1s IP seen for their $(R_f)_4PH_2$ counterparts, the N 1s IP of both TPPZn and TFPPZn is larger by 0.5 and 0.2 eV than the N1 1s IP of their respective free base analogues; the net result of this invariance of nitrogen core electrostatic potential between the $(R_f)_4PH_2$ and $(R_f)_4PZn$ systems is that the difference in N 1s IP between $(R_f)_4PZn$ and TPPZn is only ~60% as large as the analogous difference between the N1 1s core ionizations of $(R_f)_4PH_2$ and $TPPH_2$. Though the origin of this discrepancy in *meso*-substituent effects for porphyrin and (porphinato)zinc(II) species in these XPS studies is unknown, one possible hypothesis is that the strongly σ-electron-withdrawing perfluoroalkyl groups effect enhanced removal of electron density from the central zinc atom through the nitrogen atoms in the $(R_f)_4PZn$ compounds, thus exerting a leveling effect on the N 1s core electrostatic potentials. Such an explanation is consistent with the unusually short $Zn-N_{pyridyl}$ distance observed in our structure of $(C_3F_7)_4PZn\cdot py$.

(15) Electrochemical experiments show that increasing the number of electron-withdrawing moieties at the *meso*- and β-positions that are capable of π conjugating with the macrocycle does not necessarily result in augmented porphyrin ring oxidation potentials. See: Kadish, K. M.; D'Souza, F.; Villard, A.; Autret, M.; Caemelbecke, E. V.; Bianco, P.; Antonini, A.; Tagliatesta, P. *Inorg. Chem.* **1994**, *33*, 5169−5170.

(16) Hansch, C.; Leo, A.; Taft, R. W. *Chem. Rev.* **1991**, *91*, 165−195.

(17) Moore, K. T.; Goll, J. G.; Therien, M. J. Manuscript in preparation.

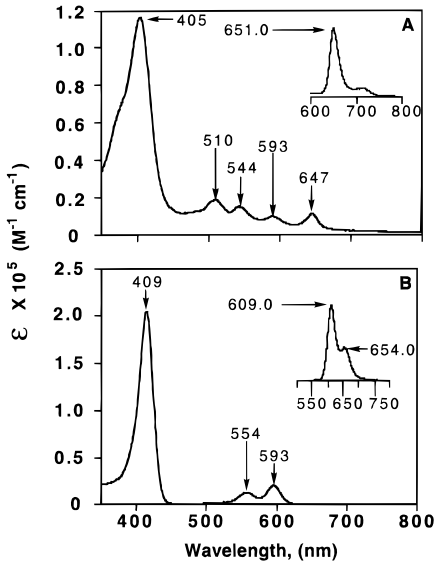

Figure 6. (A) Electronic absorption spectrum of 5,10,15,20-tetrakis-(heptafluoropropyl)porphyrin recorded in CH_2Cl_2. (B) Electronic absorption spectrum of [5,10,15,20-tetrakis(heptafluoropropyl)porphinato]zinc(II) recorded in THF. Emission spectra for these compounds are shown in the insets to the figures.

Optical Properties. As seen in Figures 6A and 6B, despite having a severely S_4-distorted structure (Figure 2), the optical spectra exhibited by $(C_3F_7)_4PH_2$ and $(C_3F_7)_4PZn$ display no unusual characteristics, such as drastically red-shifted B-bands, which are commonly observed for the well-studied 2,3,7,8,12,-13,17,18-octahalo-5,10,15,20-tetrakis(pentafluorophenyl)porphyrins and their associated zinc complexes.[1−2,12] *meso*-Tetrakis(perfluoroalkyl)porphyrins and their zinc(II)-substituted derivatives, which have no porphyrin peripheral substituents capable of π-conjugating with their distorted macrocycle cores, thus display gross electronic spectral features in common with analogous structurally unelaborated porphyrin systems.

Another striking feature of the $(R_f)_4PH_2$ ligand system is also illustrated in the optical spectrum $(R_f)_4PZn$: the relative extinction coefficients of the *Q*(0,0) and *Q*(1,0) transitions of $(C_3F_7)_4PZn$ ($\log \epsilon = 4.29$ and 4.01, respectively) contrast the analogous absorptions of TPPZn ($\log \epsilon_{Q(0,0)} = 4.09$; $\log \epsilon_{Q(1,0)} = 4.36$). Because both vibronic coupling theory and experiment show that the *Q*(1,0) transition borrows a constant amount of intensity from the B-band absorption, differences in the *Q*(1,0) and *Q*(0,0) extinction coefficients are related to the relative energies of the two singlet transitions [$^1E(a_{2u}e_g)$ and $^1E(a_{1u},e_g)$] in a Gouterman four-orbital treatment (eq 1).[18]

$$\frac{A[Q(0,0)]}{A[Q(1,0)]} = (\text{const})[^1E(a_{2u},e_g) - {}^1E(a_{1u},e_g)]^2 \qquad (1)$$

Based on their respective optical spectra, the relative energies of the $a_{2u} \rightarrow e_g$ and $a_{1u} \rightarrow e_g$ transitions of the $(R_f)_4PZn$ complexes must clearly differ from those of TPPZn; this is consistent with what was gleaned from the XPS data for these complexes, namely, that the $(R_f)_4PZn$ species evince drastically elevated electrostatic potential at the macrocycle central nitrogens with respect to TPPZn. The XPS and electronic absorption experiments carried out on the [tetrakis(perfluoroalkyl)porphinato]zinc(II) complexes are thus both consistent with a significantly stabilized a_{2u} orbital for these species; it is thus a reasonable expectation that the highest lying molecular orbital for $(R_f)_4PZn$ is of a_{1u} symmetry;[14b,19] this hypothesis has recently been borne out by complementary spectroscopic experiments.[20]

Table 5 compiles optical data obtained for the $(R_f)_4PH_2$ and $(R_f)_4PZn$ compounds reported in this study, along with that for porphine (PH_2), (porphinato)zinc(II) (PZn), $TPPH_2$, TPPZn, Br_8-$TFPPH_2$, and $Br_8TFPPZn$; the electronic absorption spectra for all these compounds were acquired in solvents appropriate to facilitate electronic structural correlations. A number of conclusions can be drawn from this comparative study. Examination of the electronic spectral data for the free-base porphyrin macrocycles shows the following: (i) The *B*(0,0) transitions (Soret bands) of the $(R_f)_4PH_2$ macrocycles appear at energies that are ~0.08 and 0.34 eV blue shifted compared to the respective *B*(0,0) transitions of $TPPH_2$ and Br_8TFPPH_2; moreover, these transitions occur at a wavelength similar to the B band of PH_2. (ii) While the energies of the $Q_{x,y}(0,0)$ and $Q_{x,y}(1,0)$ transitions are virtually invariant throughout the $(R_f)_4$-PH_2 series, these bands are (a) ~0.1 eV red shifted with respect to the analogous quasiallowed absorptions of PH_2, (b) similar in energy to those of $TPPH_2$, and (c) dramatically blue shifted (0.16−0.4 eV) relative to the Q-band absorptions of Br_8TFPPH_2. The net result of these disparate B and Q transition energies in this series of free-base porphyrin derivatives is that the spectral midpoint,[21] which is defined as the center of gravity of the B−Q transition envelope, decreases in the order $PH_2 > (R_f)_4PH_2 \sim TPPH_2 >> Br_8TFPPH_2$. The greater spectral midpoint energy for PH_2 with respect to the $(R_f)_4PH_2$ species derives from the fact that its Q-band absorptions are blue shifted with respect to those of the *meso*-tetrakis(perfluoroalkyl)porphyrins; the magnitude of the *B*(0,0) − *Q*(0,0) spectral splitting thus decreases in the order $(R_f)_4PH_2 > PH_2 > TPPH_2 >> Br_8TFPPH_2$.

The nearly 1.0 eV difference in energy between the *B*(0,0) and *Q*(0,0) absorptions for the $(R_f)_4PH_2$ compounds is the largest ever observed for free-base porphyrin derivatives. This extensive *B*(0,0)−*Q*(0,0) splitting results directly from the much larger electron correlation[22] for porphyrins that bear *meso*-perfluoroalkyl groups: relative to $TPPH_2$, $(R_f)_4PH_2$ species have minimal faculty to participate in delocalization of porphyrin π-centered electron density. What is particularly amazing is the fact that the $(R_f)_4PH_2$ compounds exhibit a larger electron correlation than that observed for even PH_2! While it is not possible at this time to attribute a genesis for this behavior, this result may follow from our XPS data, which shows that *meso*-perfluoroalkyl moieties are particularly effective in removing electron density from the porphyrin nitrogen atoms. This enhanced electron correlation observed in the *meso*-tetrakis(perfluoroalkyl)porphyrins strongly suggests that substitution of one or more of the 2, 3, 7, 8, 12, 13, 17, and 18 positions of the $(R_f)_4$-PH_2 macrocycles will define porphyrin ligands in which magnified Hammett−Taft substituent effects are exhibited; moreover these porphyrins should display extreme sensitivity to both β-substituent field and resonance properties, perhaps greater than that seen for any other tetra(*meso*-substituted)-porphyrin yet studied.

With respect to the optical data for the (porphinato)zinc(II) derivatives listed in Table 5, similar conclusions can be drawn.

(18) (a) Spellane, P. J.; Gouterman, M.; Antipas, A.; Kim, S.; Liu, Y. C. *Inorg. Chem.* **1980**, *19*, 386−391. (b) Perrin, M. H.; Gouterman, M.; Perrin, C. L. *J. Chem. Phys.* **1969**, *50*, 4137−4150; erratum, *Ibid.* **1972**, *56*, 2492.

(19) Barzilay, C. M.; Sibilia, S. A.; Spiro, T. G.; Gross, Z. *Chem. Eur. J.* **1995**, *1*, 222−231.

(20) Moore, K. T.; Angiolilo, P. J.; Therien, M. J. Manuscript in preparation.

(21) Binstead, R. A.; Crossley, M. J.; Hush, N. S. *Inorg. Chem.* **1991**, *30*, 1259−1264.

(22) Gouterman, M. In *The Porphyrins*, Dolphin, D., Ed.; Academic Press: London, 1978; Vol. III, pp 1−165.

(23) (a) Quimby, D. J.; Longo, F. R. *J. Am. Chem. Soc.* **1975**, *97*, 5111−5117. (b) Bonnett, R.; Harriman, A.; Kozyrev, A. N. *J. Chem. Soc., Faraday Trans.* **1992**, *88*, 763−769.

Table 5. Optical Spectra of [5,10,15,20-Tetrakis(perfluoroalkyl)porphinato]zinc(II) Complexes and Their Free Base Analogues: Comparative Electronic Spectroscopy as a Function of the Macrocycle Substitution Pattern

		absorption band maxima						spectral midpoint[b]	$B(0,0)-Q(0,0)$
compd[a]	solvent	$B(0,0)$ (eV)	$Q(1,0)$ (eV)		$Q(0,0)$ (eV)			(eV)	splitting, (eV)
$(CF_3)_4PZn$	THF	2.94	2.21		2.06			2.50	0.88
$(C_3F_7)_4PZn$	THF	3.01	2.24		2.09			2.55	0.92
$(C_7F_{15})_4PZn$	THF	2.97	2.22		2.08			2.52	0.89
$(CF_3)_4PH_2$	CH_2Cl_2	3.07	2.43	2.09[c]	2.27	1.91[d]		2.58[e]	0.98[f]
$(C_3F_7)_4PH_2$	CH_2Cl_2	3.05	2.43	2.10[c]	2.27	1.92[d]		2.57[e]	0.96[f]
$(C_7F_{15})_4PH_2$	1,1,2-$C_2Cl_3F_3$	3.08	2.44	2.09[c]	2.29	1.92[d]		2.59[e]	0.98[f]
PZn	THF	3.11	2.34		2.20			2.66	0.91
TPPZn	THF	2.97	2.23		2.09			2.53	0.88
Br_8TFPPZn	THF	2.72	2.13		1.98			2.35	0.74
PH_2	CH_2Cl_2	3.13	2.54	2.18[c]	2.40	2.03[d]		2.68[e]	0.94[f]
$TPPH_2$	CH_2Cl_2	2.99	2.41	2.11[c]	2.26	1.93[d]		2.54[e]	0.90[f]
Br_8TFPPH_2	CH_2Cl_2	2.73	2.27	1.97[c]	2.10	1.88[d]		2.36	0.74

[a] Abbreviations: 5,10,15,20-tetrakis(trifluoromethyl)porphyrin [$(C_3F_7)_4PH_2$]; 5,10,15,20-tetrakis(heptafluoropropyl)porphyrin [$(C_3F_7)_4PH_2$]; 5,10,15,20-tetrakis(pentadecafluoroheptyl)porphyrin [$(C_7F_{15})_4PH_2$]; [5,10,15,20-tetrakis(trifluoromethyl)porphinato]zinc(II) [$(CF_3)_4PZn$]; [5,10,15,20-tetrakis(heptafluorpropyl)porphinato]zinc(II) [$(C_3F_7)_4PZn$]; [5,10,15,20-tetrakis(pentadecafluoroheptyl)porphinato]zinc(II) [$(C_7F_{15})_4PZn$]; porphine (PH_2); (porphinato)zinc(II) (PZn); 5,10,15,20-tetraphenylporphyrin ($TPPH_2$), [5,10,15,20-tetraphenylporphinato]zinc(II) (TPPZn); 2,3,7,8,12,13,17,18-octabromo-5,10,15,20-tetrakis(pentafluorophenyl)porphyrin (Br_8TFPPH_2); and [2,3,7,8,12,13,17,18-octabromo-5,10,15,20-tetrakis(pentafluorophenyl)porphinato]zinc(II) ($Br_8TFPPZn$). [b] Defined as discussed in ref 21. [c] Values refer to the $Q_x(1,0)$ and $Q_y(1,0)$ transitions, respectively. [d] Values refer to the $Q_x(0,0)$ and $Q_y(0,0)$ transitions, respectively. [e] Defined as $[(\{Q_x(0,0) + Q_y(0,0)\}/2) + B(0,0)]/2$. Note that only the 0,0 electronic transitions are considered in a spectral center of gravity calculation. See ref 21. [f] Defined as $B(0,0) - [\{Q_x(0,0) + Q_y(0,0)\}/2]$.

Table 6. The Effect of Porphyrin Electron Withdrawing Substituents on Fluorescence Wavelength, Quantum Yield, and Lifetime of the S_1-Excited State; Photophysical Data for [5,10,15,20-Tetrakis(perfluoroalkyl)porphinato]zinc(II) Complexes and their Free Base Analogues

	fluorescent emission maxima					
compd	solvent	λ_1 (nm)	λ_2 (nm)	ϕ_F	lifetime (ns)	Stokes shift (cm^{-1})
$(CF_3)_4PZn$	THF	611	659	0.0082	0.86	249
$(C_3F_7)_4PZn$	THF	607	652	0.013	1.2	384
$(C_7F_{15})_4PZn$	THF	607	657	0.011	1.6	303
$(CF_3)_4PH_2$	CH_2C1_2	653	718	0.019	1.2	92
$(C_3F_7)_4PH_2$	CH_2C1_2	651	717	0.028	1.4	126
$(C_7F_{15})_4PH_2$	1,1,2-$C_2C1_3F_3$	650	713	0.026	1.7	102
TPPZn	THF	602	652	0.033	1.86	247
Br_8TFPPZn	THF	637	*a*	~0.0004	*b*	272
$TPPH_2$	CH_2C1_2	651	717	0.117	10.8	206
Br_8TFPPH_2	CH_2C1_2	*c*	*a*	~0	*b*	

[a] Not observed. [b] $\tau_F <$ the time resolution of our TCSPC apparatus (30 ps). [c] Quantum yield for fluorescence emission must be exceptionally small; no fluorescence emission band for this species could be detected.

Although greater disparity in the $B(0,0)$- and $Q(0,0)$-transition energies exists in the $(R_f)_4PZn$ series with respect to the $(R_f)_4PH_2$ compounds (note, for example, that the $B(0,0)$ band of $(C_3F_7)_4PZn$ lies 0.07 and 0.04 eV higher in energy than the analogous respective transitions for $(CF_3)_4PZn$ and $(C_7F_{15})_4PZn$), the B and Q bands of the $(R_f)_4PZn$ species consistently are red shifted (~0.1 eV) with respect to the analogous transitions of PZn, in common with what was observed for their respective free base derivatives. Remarkable spectral similarity is observed between the $(R_f)_4PZn$ and TPPZn complexes, while the visible transitions of these species exhibit considerable hypsochromic shifts relative to Br_8TFPPZn. A comparison of the spectral midpoints for the (porphinato)zinc(II) complexes shows a PZn > $(R_f)_4PZn$ ~ TPPZn >> Br_8TFPPZn relative energy ranking, while the $B(0,0)-Q(0,0)$ spectral splitting energies vary with $(R_f)_4PZn$ ~ PZn > TPPZn >> Br_8TFPPZn.

Photophysics. The photophysical properties relevant to the S_1-excited state of the $(R_f)_4PH_2$ and $(R_f)_4PZn$ species are presented in Table 6 along with emission, quantum yield, and fluorescence lifetime data for the compounds $TPPH_2$, Br_8TFPPH_2, TPPZn, and Br_8TFPPZn, which serve as benchmark porphyrin and (porphinato)zinc(II) chromophores for the purpose of comparison. The most significant aspect of the photophysics of the *meso*-perfluorocarbon-substituted porphyrin and (porphinato)zinc(II) derivatives is their *substantial fluorescence lifetimes*. The S_1-excited state lifetime data for the $(R_f)_4PH_2$ and $(R_f)_4PZn$ compounds stand in marked contrast to that for the well-studied 2,3,7,8,12,13,17,18-octahalo-5,10,15,20-tetrakis(pentafluorophenyl)porphyrin and [2,3,7,8,12,13,17,18-octahalo-5,10,15,20-tetrakis(pentafluorophenyl)porphinato]zinc(II) electron deficient chromophore systems: note that the fluorescent lifetimes for both Br_8TFPPH_2 and Br_8TFPPZn are drastically reduced relative to their *meso*-tetrakis(perfluoroalkyl)porphyrin analogs. This significant deactivation of the S_1 state of fluorescent porphyrins derives from spin−orbit perturbations caused by the heavy atom substituents; while such effects have been discussed extensively at both qualitative and quantitative levels,[2c,18a,22−23] the ambient temperature fluorescence properties of Br_8TFPPH_2 and Br_8TFPPZn have not previously been reported. These results, however, are consistent with work by Harriman, who has shown that two *meso*-bromo substituents are sufficient to reduce the lifetime of the porphyrin singlet-excited state to less than 50 ps.[23b]

The (0,0) and (0,1) fluorescence emission wavelengths (Table 6) of the $(R_f)_4PH_2$ and $(R_f)_4PZn$ species differ little, respectively, from those observed for $TPPH_2$ and TPPZn; the congruence of the emission energies for these electronically disparate pairs of porphyrin and (porphinato)zinc(II) compounds ensues from their nearly identical electronic absorption spectral features (Table 5). As a result, the evaluated Stokes shifts for the $(R_f)_4PH_2$ and $(R_f)_4PZn$ species differ little from those measured for $TPPH_2$ and TPPZn (Table 6). While it should be appreciated that the Stokes shifts for the $(R_f)_4PH_2$ compounds are unusually small (92 to 126 cm^{-1}), 5,10,15,20-tetrakis(perfluoroalkyl)porphyrin

excited states, like those of $TPPH_2$ and TPPZn, must experience relatively minor nuclear distortions with respect to the ground state structure. Furthermore, the similarity between the absorptive and emissive properties of the rigorously S_4-distorted $(R_f)_4PH_2$ and $(R_f)_4PZn$ compounds with their 5,10,15,20-tetraphenyl-substituted analogs is consistent with the notion that the elementary photophysical properties of porphyrinic species depend far less on macrocycle structural properties than they do on whether or not porphyrin structural perturbations from planarity can lead to enhanced π conjugation with the ring *meso* and β substituents.[1,8]

Quantum yields of fluorescence emission (ϕ_F) for the $(R_f)_4PH_2$ chromophores range between 0.019 and 0.028, constituting a 4- to 6-fold reduction of this parameter with respect to that observed for the $TPPH_2$ standard; it is important to appreciate, however, that electron-deficient Br_8TFPPH_2 has no detectable fluorescence emission. A consonantly similar diminution in the magnitude of the fluorescence quantum yields for the $(R_f)_4PZn$ complexes ($\phi_F = 0.0082-0.013$) relative to TPPZn ($\phi_F = 0.033$) is evident from the data presented in Table 6. Again, the order of the ϕ_F values for these *meso*-perfluoroalkyl-substituted (porphinato)zinc(II) compounds differs tremendously from that determined for the [2,3,7,8,12,13,17,18-octahalo-5,10,15,20-tetrakis(pentafluorophenyl)porphinato]zinc(II) benchmark: the quantum yield of fluorescence for $Br_8TFPPZn$ ($\phi_F \sim 0.0004$) is 50 times smaller than that evaluated for the $(R_f)_4PZn$ chromophores.

As seen in Table 6, the $(R_f)_4PH_2$ and $(R_f)_4PZn$ compounds have relatively long fluorescence lifetimes, and span a 0.86−1.4 ns time domain; the magnitudes of these lifetimes dwarf those of Br_8TFPPH_2 and $Br_8TFPPZn$ ($\tau_F < 20$ ps). With respect to TPPZn ($\tau_F = 1.86$ ns), the evaluated lifetimes for the $(R_f)_4PZn$ complexes ($\tau_F = 0.86-1.6$ ns) are only marginally smaller. The $(R_f)_4PH_2$ chromophores, however, exhibit fluorescence lifetimes ($\tau_F = 1.2-1.7$ ns) that differ significantly from that measured for $TPPH_2$ ($\tau_F = 10.8$ ns). Given the relative similarity of the $(R_f)_4PZn$ and TPPZn fluorescence lifetimes, it is perhaps a bit surprising that the associated $(R_f)_4PH_2$ lifetimes show a precipitous drop in τ_F with respect to that seen for $TPPH_2$. Clearly, structural studies suggest that this variance cannot be due to gross differences in macrocycle nonplanarity between the $(R_f)_4PH_2$ and $(R_f)_4PZn$ systems, since both the porphyrin and (porphinato)zinc(II) species exhibit significant S_4 distortions (*vide supra*).[1] Because one would expect spin−orbit interactions and the allowable carbon-framework-localized macrocyclic vibrational modes to be similar for porphyrin and (porphinato)zinc(II) compounds with identical peripheral substituents, if the reduced fluorescence lifetime of $(R_f)_4PH_2$ species relative to $TPPH_2$ has a vibronic genesis, it must be due to differences in the nature of the proton dynamics at the porphyrin core. Such an explanation is plausible given the significantly diminished basicity of the $(R_f)_4PH_2$ macrocycles,[1] as well as the fact that extensive $TPPH_2$ Raman data[24] show that the b_{1g} type N−H in-plane bending mode can be coupled with several vibrational modes in the 1350−1600-cm^{-1} region, including υ_{19}, υ_{20}, and particularly υ_4.[24d] Finally, for both the $(R_f)_4PH_2$ and $(R_f)_4PZn$ series, it is worth noting that the $R_f = C_3F_7$ derivatives have the largest fluorescence quantum yields, while the $R_f = C_7F_{15}$ variants exhibit the longest S_1-excited state emissive lifetimes.

(24) (a) Stein, P.; Ulman, A.; Spiro, T. G. *J. Phys. Chem.* **1984**, *88*, 369−374. (b) de Paula, J. C.; Walters, V. A.; Nutaitis, C.; Lind, J.; Hall, K. *J. Phys. Chem.* **1992**, *96*, 10591−10594. (c) Bell, S. E. J.; Al-Obaidi, A. H. R.; Hegarty, M. J. N.; McGarvey, J. J.; Hester, R. E. *J. Phys. Chem.* **1995**, *99*, 3959−3964. (d) Sato, S.; Aoyagi, K.; Kitagawa, T. *J. Phys. Chem.* **1995**, *99*, 7766−7775.

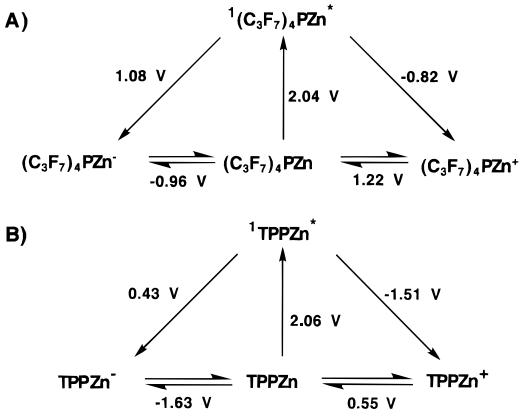

Figure 7. Modified Latimer diagrams for (A) [5,10,15,20-tetrakis-(heptafluoropropyl)porphinato]zinc(II) and (B) [5,10,15,20-tetraphenylporphinato]zinc(II). Potentials shown are with respect to NHE.

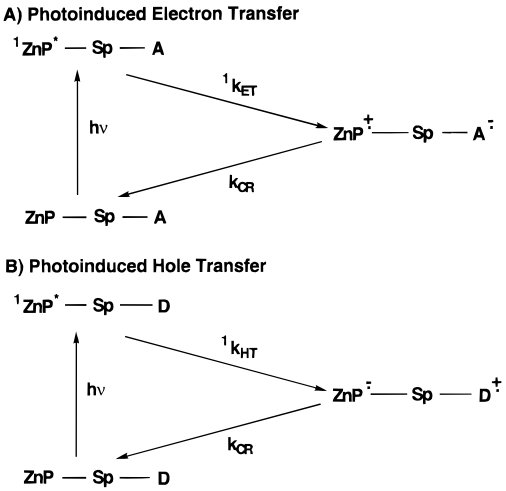

Figure 8. (A) Photoinduced electron transfer scheme based on fluorescent (porphinato)zinc(II) chromophores that feature hydrocarbon (aryl or alkyl) substituents at the porphyrin *meso* and/or β positions. (B) Photoinduced hole transfer scheme based on fluorescent [5,10,-15,20-tetrakis(perfluoroalkyl)porphinato]zinc(II) chromophores.

Despite the fact that both the magnitudes of the fluorescent lifetimes and S_1-excited state emission quantum yields of the $(R_f)_4PH_2$ and $(R_f)_4PZn$ species are diminished in comparison to both $TPPH_2$ and TPPZn chromophores, the photophysics of these *meso*-perfluorocarbon-substituted porphyrin and (porphinato)zinc(II) derivatives are more than sufficient to allow their exploitation as key components of donor−spacer−acceptor (D−Sp−A) supramolecular compounds.[25] To underscore how differently $(R_f)_4PH_2$ and $(R_f)_4PZn$ can function in such systems with respect to $TPPH_2$ and TPPZn, Figure 7A summarizes our electrochemical and photophysical data for one of the tetrakis-(*meso*-perfluoroalkyl)porphyrin chromophores, $(C_3F_7)_4PZn$, in terms of a modified Latimer diagram, which highlights both the relative reducing and oxidizing power of $(C_3F_7)_4PZn$ and its S_1-excited state, $^1(C_3F_7)_4PZn^*$. Figure 7B displays an identical diagram for the TPPZn, which along with a variety of closely related compounds figure prominently in a host of D−Sp−A systems.[25]

Congruent with their vastly divergent ground-state redox properties, $^1(C_3F_7)_4PZn^*$ and $^1TPPZn^*$ exhibit equally disparate propensities to be both oxidized and reduced. For example, Figure 7B shows that while $^1TPPZn^*$ is a strong reductant [$E°(ZnP^+/ZnP^*) = -1.51$ V] with respect to the potential of the normal hydrogen electrode (NHE), it is only a modest oxidant

(25) Wasielewski, M. R. *Chem. Rev.* **1992**, *92*, 435−461.

[$E°(ZnP^-/ZnP^*) = 0.43$ V]; this is of course consistent with the fact that ^{1}TPPZn* ordinarily functions as a reductant in photoinduced electron transfer schemes in D−Sp−A systems (Figure 8A).[25] In contrast, Figure 7A signifies that while $^1(C_3F_7)_4PZn^*$ is a good reductant [$E°(ZnP^+/ZnP^*) = -0.82$ V] with respect to NHE, it is a more impressive oxidant [$E°(ZnP^-/ZnP^*) = 1.08$ V]. The advent of $(R_f)_4PH_2$ and $(R_f)_4PZn$ compounds thus allows the possibility of accomplishing mechanistic studies of photoinduced hole transfer reactions (Figure 8B) with porphyrin-based chromophores; this is particularly important given the paucity of both strongly oxidizing, robust excited state chromophores[26] and the relative lack of detailed studies of hole tunneling events with respect to analogous electron tunneling processes.[25,27]

Summary and Conclusion

We have shown that the physical properties of tetrakis(5,10,15,20-perfluoroalkyl)porphyrin systems are unique compared to all other previously synthesized porphyrin compounds. (i) With respect to solubility, $(R_f)_4PH_2$ species exhibit drastically different properties that depend intimately on the nature of the *meso*-perfluorocarbon substituent, with $(CF_3)_4PH_2$ dissolving readily in all common organic solvents, $(C_7F_{15})_4PH_2$ appreciably soluble only in nonstandard solvents such as CFC's and fluorocarbons, and $(C_3F_7)_4PH_2$ soluble[1] in an unusually wide range of media that includes pentane, THF, aqueous methanol, CFC's, and fluorocarbons. (ii) Highly electron deficient $(R_f)_4PH_2$ and $(R_f)_4PZn$ species exhibit porphyrin ring centered electrochemical responses that differ markedly from the well-studied 2,3,7,8,12,13,17,18-octahalo-5,10,15,20-tetraphenylporphyrin systems in that they exhibit an anodic electrode-coupled redox process that is one electron in nature as well as electrochemically determined HOMO-LUMO gaps identical to their 5,10,15,20-tetraphenylporphyrin analogs. (iii) XPS studies demonstrate a remarkable enhancement of the core nitrogen 1s ionization energies, signaling a significant enhancement of nitrogen-centered electrostatic potential; these potentials differ by hundreds of millivolts from other classes of electron deficient porphyrins examined by this technique. (iv) Photophysical studies show that the S_1-excited states of the $(R_f)_4PH_2$ and $(R_f)_4PZn$ chromophores are long lived and produced at reasonably high quantum efficiency; these species are thus not subject to the types of heavy atom-induced spin−orbit perturbations that deactivate the excited states of chromophores in the similarly electron deficient 2,3,7,8,12,13,17,18-octahalo-5,10,15,20-tetraphenylporphyrin systems.

In sum, nonconjugating *meso*-perfluoroalkylporphyrin substituents stabilize the filled porphyrin π orbitals of $(R_f)_4PH_2$ and $(R_f)_4PZn$ to a similar degree with respect to what has been observed for 2,3,7,8,12,13,17,18-octahalo-5,10,15,20-tetraphenylporphyrins and their (porphinato)zinc(II) derivatives. Furthermore, the XPS data demonstrate extremely impressive electron-withdrawing effects modulated through the macrocycle σ network for the 5,10,15,20-tetrakis(perfluoroalkyl)porphyrin systems: this suggests a particular propensity for these macrocycles to abate electrostatic repulsion between filled metal $d_{x^2-y^2}$ and d_{z^2} orbitals and the nitrogen atoms of the tetradentate porphyrin ligand. Such unusual ground-state electronic features, coupled with the unrivaled redox properties of their singlet excited states, along with the straightforward ability to tailor their solubility properties, clearly establish tremendous potential of these systems for modulating porphyrin-based transition metal catalysts, developing novel supramolecular systems with unusual photophysical properties, and studying charge tunneling reactions in relatively unexplored energy regimes.

Acknowledgment. We thank the National Science Foundation (CHE93-57130) and the U.S. Department of Energy (DE-FGO2-94ER14494) for their generous support of this work. M.J.T. gratefully acknowledges the Searle Scholars Program (Chicago Community Trust), the Arnold and Mabel Beckman Foundation, and E. I. du Pont de Nemours for Young Investigator Awards, as well as the Alfred P. Sloan Foundation for a research fellowship. A.G. thanks Physical Electronics, Inc., Eden Prairie, MN, for providing access to the XPS instrumentation used in this study.

Supporting Information Available: X-ray structure determination of compound 919 and tables giving structure determination values, refined positional and thermal parameters, and bond distances for compound 919 (21 pages). See any current masthead page for ordering and Internet access instructions.

JA9610904

(26) Yam, V. W.-W.; Che C.-M. *Coord. Chem. Rev.* **1990**, *97*, 93−104.
(27) (a) Closs, G. L.; Miller, J. R. *Science (Washington, D.C.)* **1988**, *240*, 440−447. (b) Meyer, T. J. *Pure Appl. Chem.* **1990**, *62*, 1003−1009. (c) Winkler, J. R.; Gray, H. B. *Chem. Rev.* **1992**, *92*, 369−379.